

#### RESEARCH PAPER

# Synthesis and characterization of Fe<sub>3</sub>O<sub>4</sub>-activated charcoal composite of Ihau fruit peel (*Dimocarpus longan* var. malesianus Leenh.) as methylene blue adsorbent

Azizah Fithri Ananda, [a] Teguh Wirawan [a]\*, and Nanang Tri Widodo [a]

[a] Department of chemistry, Universitas Mulawarman, Kampus Gunung Kelua, Samarinda, 75119, East Kalimantan, Indonesia E-mail: twirawan@fmipa.unmul.ac.id

DOI: 10.29303/aca.v8i2.253

#### **Article info:**

Received 29/06/2025

Revised 13/10/2025

Accepted 12/11/2025

Available online 29/11/2025

Abstract: Research has been conducted on the synthesis and characterization of Fe<sub>3</sub>O<sub>4</sub>-active charcoal composite of ihau fruit peel (MAACI) as a methylene blue dye adsorbent. This research aimed to produce activated charcoal from ihau fruit peel (AACI) composited with magnetite (Fe<sub>3</sub>O<sub>4</sub>). AACI was prepared by carbonating Ihau fruit peel in a furnace at 425 °C for 1 hour and chemically activated by immersion in an HCl solution for 24 hours. The synthesis of MAACI was carried out using the coprecipitation method with FeCl<sub>3</sub>•6H<sub>2</sub>O and FeSO<sub>4</sub>•7H<sub>2</sub>O in a 3:2 ratio, followed by compounding with AACI. The MAACI was characterized by Fourier Transform Infrared (FTIR), Scanning Electron Microscopy (SEM) and X-Ray Diffraction (XRD). The characterization results showed that the FTIR spectrum exhibits an absorption peak at a wavenumber of 586.36 cm<sup>-1</sup>, indicating the presence of the Fe-O group. SEM analysis revealed that the MMACI has denser pores and a coarser texture compared to activated charcoal. Meanwhile, XRD results showed a diffraction pattern that matches the characterization of magnetite (Fe<sub>3</sub>O<sub>4</sub>). The adsorption of methylene blue by MAACI yielded optimum results at a pH of 9 with a contact time of 45 minutes. The maximum adsorption capacity obtained was 8.7014 mg/g, and the adsorption process followed the Langmuir isotherm model. This adsorption takes place spontaneously, is endothermic and occurs physically.

Keywords: Composite, Fe<sub>3</sub>O<sub>4</sub>, Active Charcoal, Ihau, Methylene Blue

**Citation:** Ananda, A. F., Wirawan, T., & Widodo, N. T. (2025) Synthesis and characterization of Fe3O4-activated charcoal composite of Ihau fruit peel (Dimocarpus longan var. malesianus Leenh.) as methylene blue adsorbent. Acta Chimica Asiana, 8(2), 662-671. https://doi.org/10.29303/aca.v8i2.253

#### INTRODUCTION

Modern industry has undergone rapid development, bringing numerous benefits to human life. However, this development has also had negative impacts, including waste generated by production Several industries that processes. have experienced significant growth, such as the textile, beauty, food, and beverage industries, often use dyes in their production processes. One commonly used dye is methylene blue, which belongs to the synthetic cationic group. Although effective in its application, methylene blue is toxic and harmful to the environment, as not all particles are absorbed during the production process. Exposure to this substance can cause various health effects, such as skin allergies, irritation, genetic mutations, and even cancer [1].

Various methods have been developed to dye waste, including adsorption coagulation-flocculation ozonization [3], membrane filtration [5], photocatalysis [6], and liquid-liquid extraction [7]. Among these methods, adsorption is the most widely used technique due to its effectiveness, low cost, and simple procedure [8]. Previous studies have utilized agricultural waste as raw material for activated carbon adsorbents, such as from salak fruit peel [9], mangosteen fruit peel [10], sukun fruit peel [11], mandarin orange fruit peel [12], and melon fruit peel [13]. The ihau fruit (Dimocarpus longan var. malesianus Leenh.), a species within the same

genus as the longan, represents a natural material with similar potential.

Ihau fruit, or cat's eye fruit, has physical and taste similarities to longan fruit. According to literature, longan fruit skin contains cellulose, hemicellulose, and lignin [14], which are important components in the formation of activated charcoal. Therefore, the ihau fruit skin also has similar content and has the potential to be used as an adsorbent material.

Activated carbon has a major drawback, namely the difficulty in separating it after use as an adsorbent. To overcome this problem, a composite was developed by adding magnetic iron oxide (Fe<sub>3</sub>O<sub>4</sub>) to activated carbon. This combination produces a new composite material that has both adsorption and magnetic properties, thereby facilitating the separation of adsorbent particles from waste liquids [15].

Based on this background, this study aims to utilize ihau fruit peel waste as a raw material for activated charcoal composite with magnetite (Fe<sub>3</sub>O<sub>4</sub>) to adsorb methylene blue dye. The physical characterization of this composite material was performed using Fourier Transform Infra Red (FTIR), Scanning Electron Microscopy (SEM), and X-Ray Diffraction (XRD). The results of this study are expected to provide an alternative to addressing environmental pollution caused by synthetic dyes.

#### **MATERIALS AND METHODS**

#### **Materials**

The equipment used in this study included Ohaus PR series analytical balances with 60 mesh sieves, vacuum pumps, Bunchner funnels, magnetic stirrers, hot plates, Thermoscientific Heratherm ovens, Kalstein furnaces, Orion Star A211 pH meters, moisture balances, sonicators, and JISICO water shakers, a Thermoscientific Orion Aquamate 8100 UV-Vis spectrophotometer, a Shimadzu Fourier Transform Infrared spectrometer, a JEOL SSM-6510 scanning electron microscope (SEM), and a Brucker Eco D8 Advance X-ray diffraction (XRD) instrument. The materials used in this study include ihau fruit peel, distilled water, methylene blue, solid FeCl<sub>3</sub>•6H<sub>2</sub>O, solid FeSO<sub>4</sub>•7H<sub>2</sub>O, 25% NH<sub>4</sub>OH, 2 M HCl, concentrated H<sub>2</sub>SO<sub>4</sub>, *n*-hexane, and NaOH.

#### Methods Preparation of Ihau Fruit Peel

The ihau fruit peel is cleaned, cut into small pieces, and dried in the sun. The ihau fruit peel is ground into a fine powder. The ihau fruit peel powder is

sieved using a 60-mesh sieve. The ihau fruit peel powder is sonicated for 15 minutes in n-hexane, and the process is repeated three times until oil is extracted. The Ihau fruit peel powder is dried in an oven at 105 °C until it is completely dry.

#### **Preparation of AACI**

The fine powder of the ihau fruit is carbonized using a furnace at a temperature of 425 °C for 1 hour. The ihau fruit shell charcoal is cooled. Seventy-five grams of ihau fruit shell charcoal powder is soaked in a 2 M HCl solution for 24 hours. The mixture is separated, the residue is washed until the pH is the same as that of distilled water, then dried in an oven at 105 °C for 1 hour and cooled. The activated charcoal is sieved using a 60-mesh sieve.

#### Preparation of Fe<sub>3</sub>O<sub>4</sub>

FeCl<sub>3</sub>:6H<sub>2</sub>O solids of 6 grams were dissolved in 100 mL of distilled water. A total of 3.9 grams of FeSO<sub>4\*</sub>7H<sub>2</sub>O was dissolved in 100 mL of hot distilled water, and then a few drops of concentrated H<sub>2</sub>SO<sub>4</sub> solution were added until the solution became lighter in colour. A FeCl<sub>3</sub> solution and a FeSO<sub>4</sub> solution were mixed while stirring with a magnetic stirrer. Then, 200 mL of a 25% NH<sub>4</sub>OH solution was added dropwise, maintaining a temperature of 70 °C for 3 hours. The mixture was filtered, and the precipitate was washed until the pH of the filtrate matched that of distilled water. Magnetite was dried in an oven at 100 °C for 3 hours and then placed in a desiccator. Magnetite was crushed and sieved using a 60 mesh sieve [16].

#### **Preparation of MAACI**

FeCl<sub>3</sub>•6H<sub>2</sub>O solids of 6 grams were dissolved in 100 mL of distilled water. A total of 3.9 grams of FeSO<sub>4</sub>•7H<sub>2</sub>O was dissolved in 50 mL of hot distilled water, and a few drops of concentrated H<sub>2</sub>SO<sub>4</sub> solution were added until the solution became lighter in colour. A FeCl<sub>3</sub> solution and a FeSO<sub>4</sub> solution were mixed while stirring with a magnetic stirrer. In another container, 10 grams of AACI was added to 100 mL of distilled water and stirred using a magnetic stirrer while being heated to 70 °C. Into the suspension, a mixture of FeCl<sub>3</sub> and FeSO<sub>4</sub> solutions, and a 25% NH<sub>4</sub>OH solution, up to 100 added dropwise, maintaining was temperature of 70 °C for 3 hours. The mixture was filtered, and then the precipitate was washed until the pH of the filtrate matched that of distilled water. The precipitate was dried in an oven at 100 °C for 3 hours and then placed in a desiccator. The AACI was crushed and sieved using a 60 mesh sieve [16].

#### Adsorbent Characterization Test

#### Fourier Transform InfraRed (FTIR)

The AACI, Fe<sub>3</sub>O<sub>4</sub>, and MAACI were analyzed using FTIR to determine the functional groups present in the AACI, Fe<sub>3</sub>O<sub>4</sub>, and MAACI.

#### Scanning Electron Microscope (SEM)

The AACI before Activation, AACI after Activation, and MAACI were analyzed using SEM to determine the surface morphology of AACI before Activation, AACI after Activation, and MAACI.

#### X-Ray Diffraction (XRD)

The AACI, Fe<sub>3</sub>O<sub>4</sub> and MAACI were analyzed using XRD to determine the structure and crystal arrangement of the AACI, Fe<sub>3</sub>O<sub>4</sub> and MAACI.

### Adsorption of Methylene Blue by MAACI

#### **Determination of Optimum pH**

The MAACI was as much as 0.05 grams and was added to 25 mL of a 5 mg/L methylene blue dye solution, whose pH had been adjusted to 3, 4, 5, 6, 7, 8, 9, and 10 by adding NaOH solution or HCl solution. The mixture was stirred using a magnetic stirrer for 30 minutes. The mixture was then separated using an external magnet, and the filtrate was analyzed for dye concentration using a UV-Vis spectrophotometer at a wavelength of 664 nm. According to Sastrawidana, adsorption efficiency is calculated using the following equation [17]:

Adsorption efficiency (%) = 
$$\frac{C_0 - C_t}{C_0} \times 100 \%$$

Description:

 $C_0$  = initial dye concentration (mg/L)

C<sub>t</sub> = final dye concentration (mg/L)

The value of adsorption capacity according to Kusumaningrum can be calculated based on the following equation [18]:

$$q_e = \frac{(C_0 - C_e)}{W} \times V$$

Description:

q<sub>e</sub> = adsorption capacity (mg/g)

 $C_0$  = initial dye concentration (ppm)  $C_e$  = final dye concentration (ppm)

W = adsorbent mass (gram)

V = Volume of solution (Liter)

#### **Determination of Optimum Time**

The MAACI was added to 25 mL of a 5 mg/L methylene blue dye solution, and the mixture was stirred using a magnetic stirrer for 5, 10, 15, 30, 45, 60, and 90 minutes, respectively. The pH of the solution was maintained at the optimum pH. The mixture was separated using an external magnet, the filtrate was determined for dye concentration using a UV-Vis spectrophotometer at a wavelength of 664 nm.

#### **Determination of Adsorption Capacity**

The MAACI was added to 25 mL of methylene blue dye solution with concentrations of 10, 20, 30, 50, 100, 150, and 200 mg/L. The L. The pH of the solution was set at the optimum pH, and it was stirred using a magnetic stirrer for the optimum time. The mixture was separated using an external magnet, and the filtrate was used to determine the concentration of methylene blue using a UV-Vis spectrophotometer at a wavelength of 664 nm. Determination of the Langmuir adsorption isotherm is written with the following equation [17]:

$$\frac{1}{q_e} = \frac{1}{K_L q_m} \frac{1}{C_e} + \frac{1}{q_m}$$

Description:

q<sub>e</sub> = adsorption capacity (mg/g)

q<sub>m</sub> = maximum adsorption capacity (mg/g)

 $K_L$  = Langmuir constant (L/mg)

C<sub>e</sub> = final concentration (mg/L)

Then, a curve can be created by plotting the relationship  $\frac{1}{q_e}$  between the y-axis  $a\frac{1}{C_e}$ nd the x-axis, allowing for the determination of the slope  $\frac{1}{K_L q_m}$  and  $intercept \frac{1}{q_m}$ . The determination of the Freundlich adsorption isotherm is written with the following equation [17]:

$$\log\log q_e = \log\log K_F + \frac{1}{n}\log\log C_e$$

Description:

q<sub>e</sub> = adsorption capacity (mg/g)

K<sub>f</sub> = Freundlich constant (mg/g)

n = adsorption intensity

C<sub>e</sub> = final concentration (mg/L)

Then, a curve can be plotted of the relationship between Log  $q_e$  on the y-axis and Log  $C_e$  on the x-axis to obtain the slope  $\frac{1}{n}$  and intercept,

Log K<sub>f</sub>. The appropriate adsorption isotherm

pattern can be determined based on the higher R<sup>2</sup> value.

#### **Determination of Adsorption Thermodynamics**

The MAACI, at a concentration of up to 0.05 grams, was added to 25 mL of a 5 mg/L methylene blue dye solution at temperatures of 30, 40, and 50 °C. The pH of the solution was adjusted to the optimum pH, and the mixture was stirred using a shaker for the optimal time. The mixture was separated using an external magnet, and the filtrate was determined for dye concentration using a UV-Vis spectrophotometer at a wavelength of 664 nm. The thermodynamics of adsorption on an adsorbent can be determined by the following equation [19]:

$$ln(K_d) = \frac{\Delta S^0}{R} + \frac{\Delta H^0}{RT}$$

#### Description:

T = solution temperature (K)

K<sub>d</sub> = thermodynamic equilibrium constant R = gas ideal constant (8.314 J/mol.K)

 $\Delta H^{\circ}$  = enthalpy change  $\Delta S^{\circ}$  = entropy change

From this equation, a curve of the relationship between  $\frac{1}{T}$  and ln  $K_d$  can be plotted, resulting in a regression equation used to determine the change value of  $\Delta H^{\circ}$  and  $\Delta S^{\circ}$ , according to the linear form of the Van't Hoff equation as follows:

$$\Delta G^{0} = -RT \ln(K_d)$$
$$\Delta G^{0} = \Delta H^{0} - T \cdot \Delta S^{0}$$

#### Description:

R = gas ideal constant (8.314 J/mol.K)

T = solution temperature (K)

K<sub>d</sub> = thermodynamic equilibrium constant

 $\Delta G^{\circ}$  = Gibbs free energy change

 $\Delta H^{\circ}$  = enthalpy change  $\Delta S^{\circ}$  = entropy change

#### **RESULTS AND DISCUSSION**

## Adsobent Characterization Test Fourier Transform InfraRed (FTIR)

The AACI, Fe $_3O_4$ , and MAACI were characterized using Fourier Transform Infrared (FTIR) spectroscopy, which aims to identify the functional groups contained therein based on their corresponding wave numbers. The results of the FTIR spectrum can be shown in Figure 1.

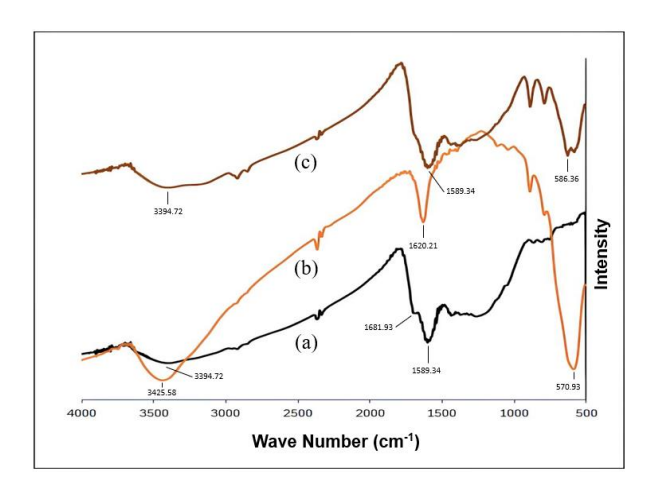


**Figure 1.** FTIR Spectrum Results of (a). AACI, (b). Fe<sub>3</sub>O<sub>4</sub> and (c). MAACI

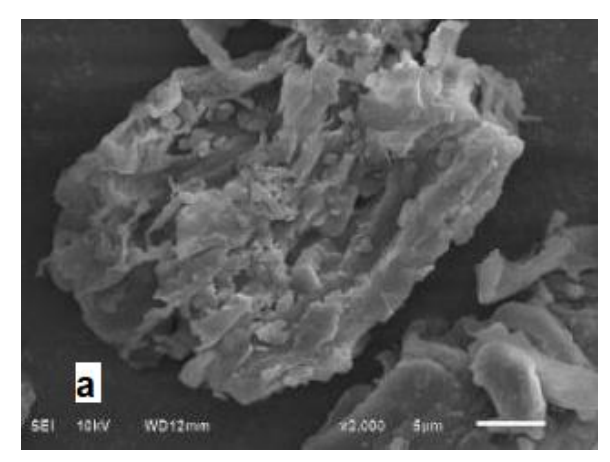
Based on the characterization test using FTIR in Figure 1, AACI shows an absorption peak at wave number 1681.93 cm<sup>-1</sup> which indicates the presence of O-H bending vibration groups, indicating the presence of hydroxyl bonds and wave number 1589.34 cm<sup>-1</sup> as a sign of the presence of C=C groups, as well as at wave number 3394.72 cm<sup>-1</sup> which shows the presence of stretching vibration groups hydrogen bonds. In Fe<sub>3</sub>O<sub>4</sub>, there is an absorption peak at wave number 1620.21 cm<sup>-1</sup>, which shows the absorption of the O-H bending vibration group as a sign of the hydroxyl bond, at wave number 3425.58 cm<sup>-1</sup>, which shows the O-H stretching vibration group as a sign of the hydrogen bond and at wave number 570.93 cm<sup>-1</sup>, which comes from the stretching vibration of the Fe-O group. Meanwhile, in the MAACI, the absorption peak at a wavenumber of 3232.70 cm<sup>-1</sup> indicates the O-H stretching vibration group, an indication of hydrogen bonding. The peak at 1589.34 cm<sup>-1</sup> suggests the presence of C=C groups, and the peak at 586.36 cm<sup>-1</sup> shows the absorption of metal oxygen in the form of Fe-O groups.

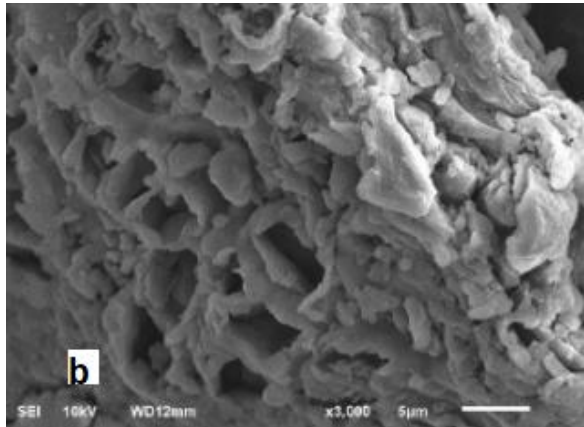
**Table 1.** Functional Group Analysis Results of AACI, Fe<sub>3</sub>O<sub>4</sub> and MAACI

Functional	Wave number (cm <sup>-1</sup> )			
Groups	AACI	Fe <sub>3</sub> O <sub>4</sub>	MAACI	
O-H bending Vibration	1681.93	1620.21		
O-H streching vibration	3394.72	3425.58	3394.72	
C=C	1589.34	-	1589.34	
Fe-O Streching		570.93	586.36	

#### Scanning Electron Microscope (SEM)

The AACI before and after Activation, as well as the MAACI, were characterized using a Scanning Electron Microscope (SEM), which aims to observe the morphology of the adsorbent surface. SEM characterization results can be seen in Figure 2.





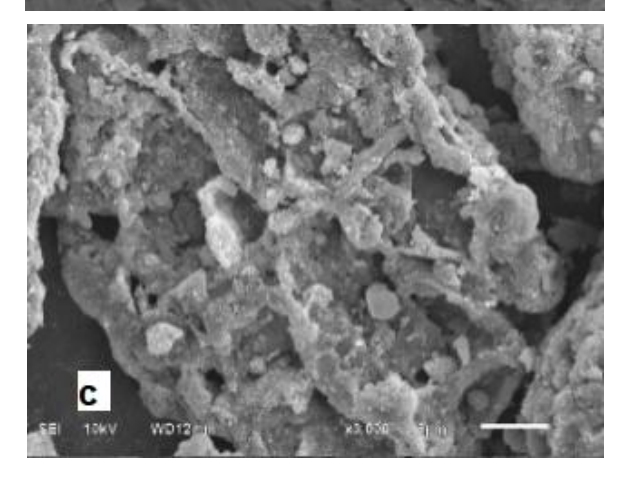


**Figure 2.** SEM Analysis Results with 3.000x Magnification (a). AACI before activation, (b). AACI after activation and (c). MAACI

Figure 2 shows that the surface of the AACI before Activation (a) is not porous with tightly bound particles, while after activation using 2 M HCI (b), the adsorbent surface becomes more porous due to the dissolution of impurities, so that the adsorbate absorption capacity increases [20]. In the MAACI (c), the pores look tighter and the surface is rougher due to the filling of spherical  $Fe_3O_4$  particles, proving the formation of the composite.

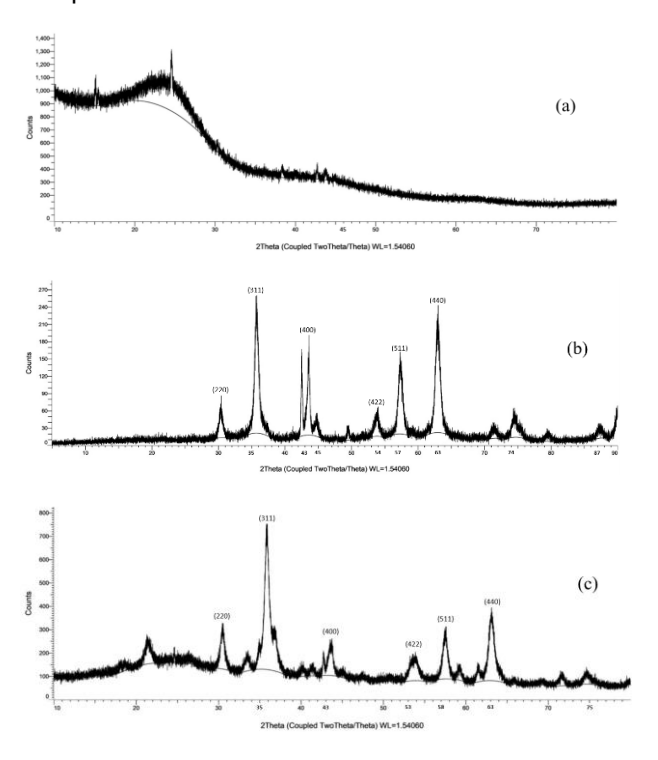


**Figure 3.** XRD Diffraction Peak Identification Results (a). AACI, (b). Fe<sub>3</sub>O<sub>4</sub> and (c). MAACI

#### X-Ray Diffraction (XRD)

The crystal structures of the AACI, Fe<sub>3</sub>O<sub>4</sub>, and MAACI were characterized using X-ray Diffraction (XRD) to determine the structure and arrangement of the crystals formed on the adsorbent. The results of XRD characterization can be seen in Figure 3.

Based on Figure 3, the characterization test results indicate that the mineral in the MAACI exhibits a diffraction pattern similar to that of magnetite (Fe<sub>3</sub>O<sub>4</sub>). The presence of sharp peaks in the diffractogram shows that the Fe<sub>3</sub>O<sub>4</sub> material is crystalline. The observed diffraction angles are in accordance with the JCPDS No. 19-0629 standard for the magnetite (Fe<sub>3</sub>O<sub>4</sub>) phase, specifically at angles of 30.095°, 35.422°, 43.052°, 53.391°, 56.942°, 62.515°, and 73.948°. Meanwhile, AACI

showed wider diffraction peaks, indicating an amorphous nature. After compositing with iron oxide, additional diffraction peaks appear that follow the typical pattern of Fe<sub>3</sub>O<sub>4</sub>. These characterization results suggest that the compositing process of AACI with Fe<sub>3</sub>O<sub>4</sub> material has been successful.

#### Adsorption of Methylene Blue by MAACI

#### **Determination of Optimum pH**

In this study, the effect of pH variation on the adsorption performance of MAACI in adsorbing methylene blue was analyzed to determine the optimum pH. The relationship between pH variation and the adsorption efficiency (%) of methylene blue dye is presented in Figure 4.

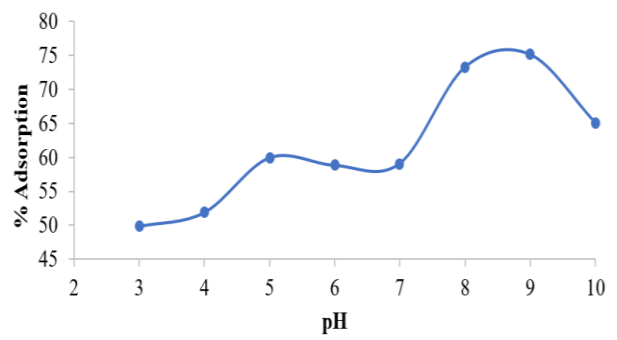


**Figure 4.** Effect of pH Variation on the Amount of Methylene Blue Adsorbed by MAACI

Based on the figure above, it is evident that the optimum pH is achieved at pH 9, with a corresponding adsorption efficiency of 75.15%. These results indicate that the MAACI has the best performance as an adsorbent at that pH. This finding aligns with Wati's research, which suggests that pH 9 is the optimal condition for the methylene blue adsorption process, as the dye exhibits maximum adsorption efficiency in an alkaline environment [21]. Each adsorbent has different surface charge characteristics, indicating the occurrence of electrostatic interactions between the adsorbent and the adsorbate. Under acidic conditions, dye molecules are deprotonated. At the same time, the adsorbent surface tends to be when in solution, resulting electrostatic interactions that facilitate the transfer of dye to the adsorbent surface. Conversely, under alkaline conditions, an increase in OH concentration causes the adsorbent surface to become more negatively charged. It strengthens the electrostatic attraction force towards positively charged methylene blue (MB+) ions, thereby increasing the amount of adsorbed dye [22].

#### **Determination of Optimum Time**

In this study, adsorption tests were conducted with varying times to determine the optimum time for the MAACI to adsorb methylene blue dye. The graph of time variation against the adsorption capacity of methylene blue dye can be seen in Figure 5.

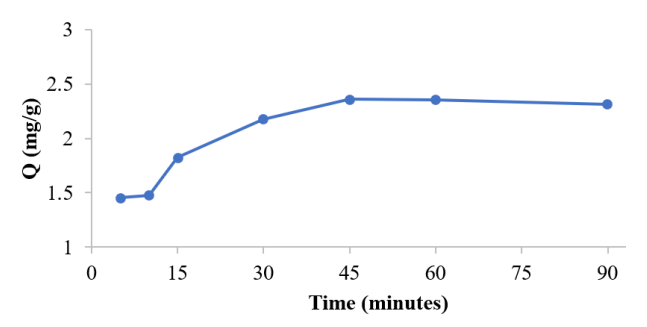


**Figure 5.** Effect of Time Variation on the Amount of Methylene Blue Adsorbed by MAACI

Figure 5 shows that the optimum time for the adsorption process of methylene blue dye using MAACI occurred at 45 minutes, with an adsorption capacity of 2.3593 mg/g. After that time, there was no significant change, either an increase or a decrease in adsorption capacity. This condition indicates a desorption process, where all pores on the adsorbent have been filled, thus preventing further adsorption. Therefore, it can be concluded that the longer the contact time, the more methylene blue molecules that can be adsorbed until the saturation point is reached [23].

#### **Determination of Adsorption Capacity**

In this study, the maximum adsorption capacity of a methylene blue dye solution was determined by varying the concentration, aiming to assess the ability of MAACI in adsorbing methylene blue dye. The relationship between concentration variation and the adsorption capacity of the methylene blue dye can be seen in Figure 6.

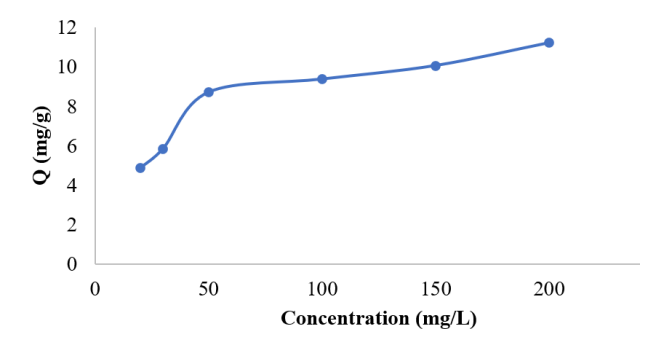


**Figure 6.** Effect of Concentration Variation on the Amount of Methylene Blue Adsorbed by MAACI

Based on Figure 6, the increase in methylene blue dye concentration is directly proportional to the increase in adsorption capacity produced. It is due to the higher concentration of methylene blue compounds in the solution, which allows more adsorbate molecules to be absorbed by the MAACI, thereby increasing the adsorption capacity (in mg/g). The optimum concentration was reached at 50 mg/L with an adsorption capacity of 8.7014 mg/g. Increasing the concentration above this value did not show a significant increase in adsorption capacity. This condition indicates desorption, which suggests that the pores in the MAACI are saturated, thereby preventing further adsorption [23]. The results of this concentration variation data can be used to determine the most suitable adsorption isotherm model. According to the literature, at low concentrations, only a small portion of the active site is occupied by methylene blue, allowing adsorption to continue until equilibrium is reached. This absorption process occurs due to electrostatic interactions between methylene blue molecules and the adsorbent surface [21]. Based on the calculation results, the maximum adsorption capacity of methylene blue dye by MAACI is 8.3270 mg/g.

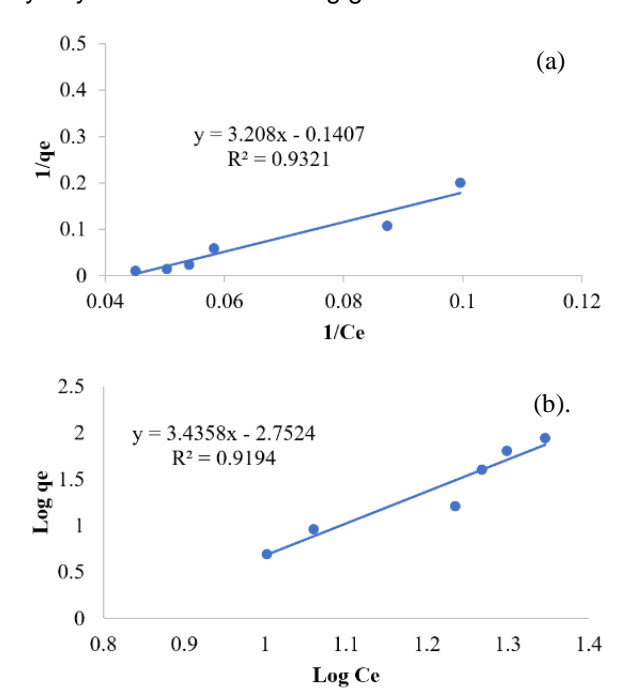


**Figure 7.** (a) Isotherm Langmuir (b) Isotherm Freundlich

#### **Adsorption Isotherm**

In this study, two isotherm models were employed: the Langmuir isotherm model and the Freundlich isotherm model, which aim to determine the nature of the interaction between the adsorbate and the adsorbent. Langmuir and the Freundlich isotherm curves, based on the regression equation for methylene blue dye adsorption by MAACI, are shown in Figure 7.

A suitable adsorption isotherm model can be determined by the correlation coefficient (R²) value, which is close to 1. Based on Figure 7, a linearity comparison between the two adsorption isotherm models was obtained, where the Langmuir model showed a higher level of fit than the Freundlich model. The R² value of the Langmuir model, 0.9321, is higher than that of the Freundlich model, 0.9194. Adsorption that follows the Langmuir model suggests that the methylene blue adsorption process by MAACI occurs in a monolayer (single layer) on a homogeneous surface, where each active site can accommodate only one such molecule [24].

#### **Determination of Adsorption Thermodynamics**

In this study, adsorption tests were carried out with temperature variations, which aimed to determine the thermodynamics of adsorption using MAACI against methylene blue dye. The relationship between temperature variation and the adsorption capacity of methylene blue dye by MAACI can be seen in Figure 8.

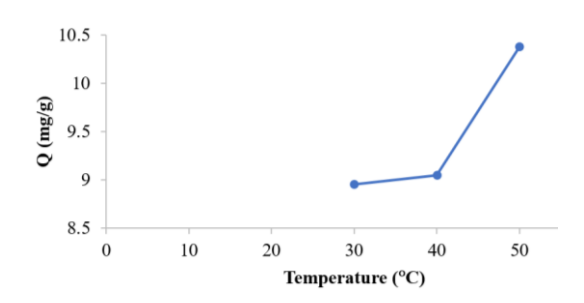


**Figure 8.** Effect of Temperature on the Amount of Methylene Blue Adsorbed by MAACI

Figure 8 shows that the adsorption capacity of methylene blue dye increases with increasing temperature. The highest adsorption capacity by MAACI occurs at 50°C with a value of 10.3806 mg/g. It shows that higher temperatures can accelerate the adsorption process, allowing more methylene blue molecules to be absorbed. Increasing the temperature can enhance the adsorption capacity by accelerating the diffusion of dye molecules into the pores of the adsorbent and strengthening the interaction between the dye molecules and the active sites on the adsorbent surface. The data from the temperature variation

graph can be used to calculate the thermodynamic parameters of the methylene blue adsorption process using the MAACI method, as shown in Table 2.

**Table 2.** Results of Temperature Variation of Methylene Blue Adsorption by MAACI

Temperature (°C)	Final Concentration (C <sub>e</sub> ) (mg/L)	Qe	$K_d = \frac{Q_e}{C_e}$	ln K <sub>d</sub>	1/T (K)
30	1.4187	1.7906	1.2621	0.2327	0.0032
40	1.3816	1.8091	1.3094	0.2696	0.0031
50	0.8477	2.0761	2.4490	0.8957	0.0030

Based on Table 2, a chart of the relationship between 1/T and In Kd on the methylene blue dye solution by MAACI can be seen in Figure 9.

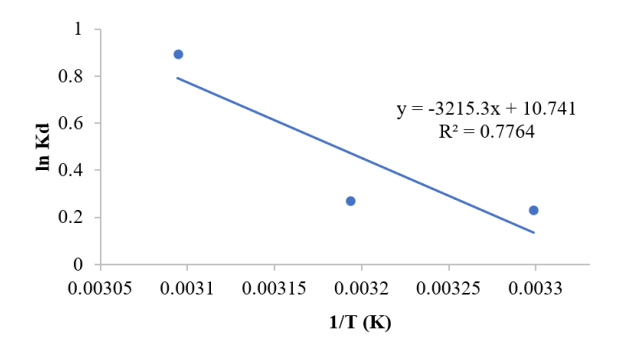


**Figure 9.** Relationship Chart of In Kd dan 1/T for Methylene Blue Adsorbed by MAACI

Figure 9 shows the linearity of the data against the linear form of the Van't Hoff equation ( $R^2 = 0.7764$ ). From the equation of the relationship curve of ln Kd dan 1/T, the thermodynamic parameters can be determined with the aim of knowing the changes in internal energy that occur in the process of adsorption of methylene blue dye with MAACI, namely enthalpy change ( $\Delta H^{\circ}$ ), entropy change ( $\Delta S^{\circ}$ ) and Gibbs free energy change ( $\Delta G^{\circ}$ ), The results can be seen in Table 3.

**Table 3.** Thermodynamic Parameters of Methylene Blue Adsorption by MAACI

	Thermodynamics Parameters			
Temperature	ΔG	ΔΗ	ΔS	
(K)	(J/mol)	(J/mol)	(J/K/mol)	
303.15	586.703			
313.15	701.981	26.273	89.3007	
323.15	2406.471			

Based on Table 3, the magnitude of  $\Delta G^{\circ}$ is negative,  $\Delta H^{\circ}$  is 26.732,0042 J/mol and  $\Delta S^{\circ}$  is 89,3007 J/K.mol. The Gibbs free energy changes  $(\Delta G^{\circ})$  are all negative, indicating that the adsorption of methylene blue dye by MAACI takes place spontaneously. The enthalpy change ( $\Delta H^{\circ}$ ) is positive, indicating that the adsorption of methylene blue dye by MAACI occurs endothermically. That is, the adsorption capacity at the same initial increases concentration with increasing temperature. The ΔH° value of less than 40 kJ/mol suggests that the adsorption is physical adsorption (physisorption). Meanwhile, a positive entropy change ( $\Delta S^{\circ}$ ) indicates an increase in system disorder, especially between the adsorbent surface and adsorbate molecules during the adsorption process [25].

#### CONCLUSION

Characterization of AACI, Fe<sub>3</sub>O<sub>4</sub>, and MAACI using FTIR, SEM, and XRD demonstrated the successful synthesis of the composite. FTIR results showed that AACI had no absorption peak in the range of 500-700 cm<sup>-1</sup>, indicating the absence of Fe-O groups. In contrast, Fe<sub>3</sub>O<sub>4</sub> and MAACI showed 586.36 at 570.93 cm<sup>-1</sup> and respectively, indicating the presence of Fe-O groups. SEM images revealed morphological changes from a tight surface on AACI before Activation to a porous one after activation. In contrast, the MAACI showed more compact pores and a rough texture due to pore filling by spherical magnetite particles. XRD analysis revealed that the diffraction pattern of the composites matched that of magnetite, indicating the successful formation of the composites. The adsorption of methylene blue by the MAACI was found to be optimal at a pH of 9 and a contact time of 45 minutes, with a maximum capacity of 8.7014 mg/g. adsorption adsorption process follows the Langmuir isotherm model ( $R^2 = 0.9321$ ), indicating that adsorption occurs in a monolayer, is physically and spontaneously adsorbed, and is an endothermic process.

#### REFERENCES

[1] Ramadhani, E. D., & Kurniawati, D. (2021). Effect of contact time and agitation speed on the adsorption process of methylene blue dyes using longan shell (Euphoria longan L.) as biosorbent. American Journal of Engineering and Applied Sciences, 4(6), 143-149..

- [2] Sari, R. A. K., Wirawan, T. & Sitorus, S. (2024). Adsorpsi Zat Warna dari Air Limbah Industri Rumah Tangga Sarung Tenun Samarinda Seberang dengan Menggunakan Adsorben dari Arang Aktif Serbuk Kulit Buah Lai (Durio Kutejensis (Hassk.) Becc.). Jurnal Atomik, 9(1), 1-8.
- [3] Raj, S., Singh, H., & Bhattacharya, J. (2023). Treatment of textile industry wastewater based on coagulation-flocculation aided sedimentation followed by adsorption: Process studies in an industrial ecology concept. Science of The Total Environment, 857, 159464.
- [4] Herfiani, Z. H., Rezagama, A. & Nur, M. (2017). Pengolahan Limbah Cair Zat Warna Jenis Indigosol Blue (C.I Vat Blue 4) sebagai Hasil Produksi Kain Batik Menggunakan Metode Ozonasi dan Adsorpsi Arang Aktif Batok Kelapa Terhadap Parameter COD dan Warna. Jurnal Teknik Lingkungan, 6(3), 1-10.
- [5] Wu, T., Yang, G., Cao, J., Xu, Z., & Jiang, X. (2022). Activation and adsorption mechanisms of methylene blue removal by porous biochar adsorbent derived from eggshell membrane. *Chemical Engineering Research and Design*, 188, 330-341.
- [6] Sugandi, D., Wahyuni, N. & Rahmalia, W. (2024). Photocatalytic Degradation of Methylene Blue by Floating TiO<sub>2</sub>-Coconut Fiber. Acta Chim. Asiana, 7(1), 437-443.
- [7] Asiah, N., Sylvia, N. & Bahri, S. (2022). Adsorpsi Zat Warna Methylene blue Menggunakan Adsorben dari Ampas Teh pada Kolom. Chemical Engineering Journal, 2(2), 75-86.
- [8] Canli, M., Abali, Y., & Bayca, S. U. (2013). Removal of methylene blue by natural and Ca and K-exchanged zeolite treated with hydrogen peroxide. Physicochemical Problems of Mineral Processing, 49.
- [9] Prabawati, S. Y., Aji, D. P. & Rahmadhani, D. (2024). Limbah Kulit Buah Salak Teraktivasi Asam Klorida sebagai Arang Aktif Logam Berat Timbal Pb(II) dan Kromium Cr(VI). Jurnal Kimia (Journal Of Chemistry), 18(1), 86-98.
- [10] Haura, U., Razi, F. & Meilina, H. (2017). Karakterisasi Adsorben dari Kulit Manggis dan

- Kinerjanya pada Adsorpsi Logam Pb(II) dan Cr(VI). *Biopropal Industri*, 8(1), 47-54.
- [11] Younas, F., Younas, S., Bibi, I., Farooqi, Z. U. R., Hameed, M. A., Mohy-Ud-Din, W., Niazi, N. K. (2024). A critical review on the separation of heavy metal (loid) s from the contaminated water using various agricultural wastes. *International journal of phytoremediation*, 26(3), 349-368.
- [12] Muflih, F., Febrina, L. & Mulyawati, I. (2023). Pemanfaatan Limbah Kulit Jeruk Mandarin sebagai Adsorben Zat Warna Methylene Blue. Sustainable Environmental and Optimizing Industry Journal, 5(1), 46-55.
- [13] Mohadi, R., Normah, Fitri, E. S. & Palapa, N. R. Unique Adsorption Properties of Cationic Dyes Malachite Green and Rhodamine-B on Longan (Dimocarpus longan) Peel. Science and Technology Indonesia, 7(1), 115-125.
- [14] Martini, S. & Yuliwati, E. (2019). Pengaruh Proses Aktivasi Terhadap Kinerja Adsorben Organik dari Kulit Buah Melon dalam Menyerap Ion Logam Cr(III) dari Limbah Cair Industri. *Distilasi*, 4(2), 33-40.
- [15] Rahmawati, I. S., Widyanto, R. M., Maulidiana, A. R., Madani, M. S. & Riski, C. N. (2022). Aktivitas Antioksidan dan Antibakteri Ekstrak Etanol Buah Ihau (Dimocarpus longan var. malesianus Leenh.) Terhadap Bakteri Gram Positif (Staphylococcus aureus). Jurnal al-azhar indonesia seri sains dan teknologi, 7(2), 138.
- [16] Reknosari, E., Wirawan, T. & Koesnarpadi, S. (2020). Adsorpsi Fenol Menggunakan Adsorben Komposit Fe<sub>3</sub>O<sub>4</sub>-Arang Aktif Ampas Kopi. *Jurnal Kimia Mulawarman*, 18(1), 30-37.
- [17] Sun, K., Leng, C. Y., Jiang, J. C., Bu, Q., Lin, G. F., Lu, X. C., & Zhu, G. Z. (2017). Microporous activated carbons from coconut shells produced by self-activation using the pyrolysis gases produced from them, that have an excellent electric double layer performance. New Carbon Materials, 32(5), 451-459.
- [18] Kusumaningrum, D. I. P., Sudarni, D. H. A. & Wahyuningsih, S. (2022). Optimasi Pengaruh Waktu Kontak dan Dosis Adsorben Limbah Daun Kayu Putih (Melaleuca cajuputi) dengan Metode Isoterm Adsorpsi Langmuir. *Jurnal Teknik Kimia USU*, 11(2), 72-79.

- [19] Neolaka, Y. A. B., Lawa, Y., Naar, J. N., Nubatonis, Y. K. & Riwu, A. A. P. (2019). Studi Termodinamika Adsorpsi Pb(II) Menggunakan Adsorben Magnetik GO-Fe<sub>3</sub>O<sub>4</sub> yang Disintesis dari Kayu Kusambi (Schleichera oleosa). *Jurnal Saintek Lahan Kering*, 2(2), 49-51.
- [20] Sam, R. F., Wirawan, T. & Aziz, A. (2024). Adsorpsi Zat Warna Rhodamine B Menggunakan Serbuk Kulit Buah Lai (Durio kutejensis (Hassk.) Becc.) Sebagai Adsorben. Jurnal Atomik, 9(2), 96-104.
- [21] Wati, A. M., Mahatmanti, F. W. & Prasetya, J. A. T. (2022). Adsorpsi Metilen Biru oleh Abu Layang Batu Bara yang Teraktivasi Menggunakan Proses Hidrotermal dengan Bantuan Gelombang Mikro. *Jurnal Penelitian Kimia*, 18(1), 58-69.
- [22] Herawati, D., Santoso, S. D. & Amalina, I. (2018). Kondisi Optimum Adsorpsi-Fluidisasi Zat Warna Limbah Tekstil Menggunakan Adsorben Jantung Pisang. *Jurnal SainHealth*, 2(1), 1-7.
- [23] Huda, T. & Yulitaningtyas, T. K. (2018). Kajian Adsorpsi Methylene Blue Menggunakan Selulosa dari Alang-Alang. *Indonesian Journal* of Chemical Analysis (IJCA), 1(01), 9-19.
- [24] Giusto, L. A., Pissetti, F. L., Castro, T. S., & Magalhães, F. (2017). Preparation of activated carbon from sugarcane bagasse soot and methylene blue adsorption. Water, Air, & Soil Pollution, 228(7), 249.
- [25] Eldamarawy, Y. A. E., Assaad, F. F., Youssef, R. A. E., & Mubarak, D. M. (2019). Adsorption Thermodynamics of Cu-Ca Ion Exchange on Nano-montmorillonite Clay System. Egyptian Journal of Chemistry, 62(Special Issue (Part 1) Innovation in Chemistry), 293-300.